

# Polyetheramide Templated Synthesis of Monodisperse $\text{Mn}_3\text{O}_4$ Nanoparticles with Controlled Size and Study of the Electrochemical Properties

Lin He<sup>1</sup>, Geng Zhang<sup>1</sup>, Yuanzhu Dong<sup>1</sup>, Zhenwei Zhang<sup>2</sup>, Shihan Xue<sup>1</sup>, Xingmao Jiang<sup>1,\*</sup>

(Received 05 October 2013; accepted 03 December 2013; published online 06 January 2014)

**Abstract:** Monodisperse  $\text{Mn}_3\text{O}_4$  nanoparticles were prepared solvothermally starting from manganese acetate by using polyether amide block copolymers (Pebax2533) as a template in isopropanol. The diameter of the nanoparticles in the range of 8.7 nm~31.5 nm was decreased with increase of Pebax2533 concentration. The electrochemical properties and application in supercapacitor of  $\text{Mn}_3\text{O}_4$  nanoparticles were further studied. The results showed that smaller nanoparticles had a larger capacitance. The higher capacitance of 217.5 F/g at a current density of 0.5 A/g was obtained on 8.7 nm  $\text{Mn}_3\text{O}_4$  nanoparticles. The specific capacitance retention of 82% was maintained after 500 times of continuous charge-discharge cycles.

**Keywords:**  $\text{Mn}_3\text{O}_4$ ; Templating; Pebax2533; Solvothermal synthesis; Supercapacitor

**Citation:** Lin He, Geng Zhang, Yuanzhu Dong, Zhenwei Zhang, Shihan Xue and Xingmao Jiang, "Polyetheramide Templated Synthesis of Monodisperse  $\text{Mn}_3\text{O}_4$  Nanoparticles with Controlled Size and Study of the Electrochemical Properties", Nano-Micro Lett. 6(1), 38-45 (2014). <http://dx.doi.org/10.5101/nml.v6i1.p38-45>

## Introduction

Supercapacitor, also known as electrochemical capacitor, is an electrochemical energy storage element which stores electrical energy based on electrode/electrolyte interface with almost no energy loss in the process. The highest energy conversion efficiency can be up to 98%, and the storage capacity of a single supercapacitor can reach thousands of Farads, 3-4 orders of magnitude higher than normal capacitors [1]. Thus, it is of great significance to develop high-performance supercapacitors in new energy area.

The key to high-performance supercapacitor is to develop materials with desired morphology, structure, size, as well as surface area. However, previous researches on electrode materials are mainly focused on carbon materials and noble metal oxides [2]. However, the noble metal oxides, such as  $\text{RuO}_2$  and  $\text{IrO}_2$  were suffered from the high cost due to the scarce resources.

$\text{Mn}_3\text{O}_4$  is a widely used precursor for magnetic materials (e.g., Mn-Zn ferrite [3]) and Li-Mn-O electrode materials for the secondary battery [4]. Besides,  $\text{Mn}_3\text{O}_4$  has also been extensively used as a catalyst in the oxidation of carbon monoxide [5], selective reduction of nitrobenzene [6], ammonization reaction of nitric oxide [7] and so on. In addition, as a cheap and commercial available transition metal oxide,  $\text{Mn}_3\text{O}_4$  has become one of the ideal choices of electrode materials for supercapacitors [8].

There are many ways available for  $\text{Mn}_3\text{O}_4$  preparation, such as meteorological growth [9], radiation [10], electric arc furnace [11], co-precipitation [12], and hydrothermal/solvothermal synthesis [13]. Among them, hydrothermal/solvothermal method possesses advantages of mild reaction condition and well-controlled size, morphology and structures, which has been adopted successfully in the synthesis of various nanometer-sized oxides, metals, semiconductors and magnetic compos-

<sup>1</sup>Changzhou University, Changzhou 213164, China

<sup>2</sup>Nanjing University of Technology, Nanjing 210009, China

\*Corresponding author. E-mail: [jxm@cczu.edu.cn](mailto:jxm@cczu.edu.cn)

ites [14,15].

Pebax2533 (poly (ether-b-amide12)) is a cheap and commercial available block copolymer. It has a wide range of applications in CO<sub>2</sub> separation [16], ethanol separation and purification [17], gas purification [18], etc. The structure unit of Pebax consists of dodecyl amide and ether components, wherein the rigid hydrophobic amides and flexible hydrophilic ether fragments make Pebax a unique template for hydrothermal/solvothermal synthesis of nanoparticles. It was shown that Pebax with high concentration favored multiple localized nucleation events, facilitating the smaller, high surface area and uniform nanocrystallites [19]. The higher viscosity of Pebax-isopropanol solution, the smaller nanoparticles can be obtained and it is harder for nanoparticles to be aggregated [20].

Herein, we prepared Mn<sub>3</sub>O<sub>4</sub> nanoparticles with different diameters by using solvothermal method with Pebax2533 block copolymer as a template. To the best of our knowledge, this synthetic pathway for Mn<sub>3</sub>O<sub>4</sub> nanoparticles has not been reported. Electrochemical performances of the Mn<sub>3</sub>O<sub>4</sub> nanoparticles were characterized by cyclic voltammetry and galvanostatic charge-discharge measurements for supercapacitor application.

## Experimental

In this study, all chemicals used were of analytical grade without further purification. Mn(CH<sub>3</sub>COO)<sub>2</sub>·4H<sub>2</sub>O (>99%) and the bulk Mn<sub>3</sub>O<sub>4</sub> (Mn>71%) were purchased from Aldrich; CH<sub>3</sub>CH<sub>2</sub>OH (>99.7%) was supplied by Shanghai Zhenxing Company; (CH<sub>3</sub>)<sub>2</sub>CHOH (>99%) was procured from Shanghai Lingfeng; Pebax2533 (poly(ether-b-amide12)) came from Shanghai Jvlu.

### Synthesis of Mn<sub>3</sub>O<sub>4</sub> nanoparticles

First, 10 g Pebax2533 was added into 40 mL anhydrous isopropanol, and the mixture was stirred at 75°C over night to give a Pebax solution at concentration of 24.2 wt%. Then, manganese acetate (4 g) dissolved in 12 mL anhydrous ethanol was mixed with the above Pebax2533 solution and poured into a stainless steel autoclave kept at 180°C over 3 days, promoting hydrolysis and condensation reactions of the manganese precursors and resulting in a transparent viscous Mn<sub>3</sub>O<sub>4</sub>/Pebax gel. The gel was washed several times to remove Pebax by using 30 mL isopropanol at 80°C and centrifuged at 8000 rpm for 3 min. After vacuum drying, a white fine powder was obtained and named as sample **a**. Sample **b** was prepared under the same conditions except that the 2.5 g Pebax2533 was used, i.e., the concentration of Pebax was 7.4 wt%.

### Structure and morphology characterization

The crystal structure of the samples was identified by X-ray diffraction (XRD, Rigaku D/max 2500PC) using Cu K<sub>α</sub> radiation. The morphology and composition of samples was observed by transmission electron microscope (TEM&EDS, JEOL JEM-2100). The specific surface area of Mn<sub>3</sub>O<sub>4</sub> nanoparticles was measured by Brunaur-Emmett-Teller (BET, Quantachrome, Autosorb-iQ2-MP). The oxidation state of the Mn<sub>3</sub>O<sub>4</sub> nanoparticles was analyzed by X-ray photoelectron spectroscopy (XPS, Thermo Scientific, ESCALAB 250Xi) using Al K<sub>α</sub> radiation.

### Preparation of electrode and electrochemical characterizations

The Mn<sub>3</sub>O<sub>4</sub> electrode was prepared as follows. A conducting agent of acetylene black (20 wt%) and a binder of polytetrafluorethylene (PTFE, 5 wt%) was mixed with Mn<sub>3</sub>O<sub>4</sub> nanoparticles (75 wt%). The mixture was milled to a homogeneous gel and pressed into a nickel foam (1 cm × 1 cm) current collector under a pressure of 10 MPa. All electrochemical measurements were carried out in a three-electrode system at room temperature. In the three-electrode, a platinum plate (1 cm × 1 cm), a mercury/mercury oxide electrode (Hg/HgO) and Mn<sub>3</sub>O<sub>4</sub> electrode was used as the counter electrode, reference electrode and working electrode, respectively. The electrolyte was 6 M KOH aqueous solution. All electrode potentials were given versus Hg/HgO electrode.

The electrochemical properties of the Mn<sub>3</sub>O<sub>4</sub> electrode were characterized on an electrochemical workstation (CHI760D, Shanghai, Chenhua) by cyclic voltammetry (CV) and galvanostatic charge-discharge experiments. The CV was carried out in a potential range from 0.0 V to 0.6 V at different scan rates. The galvanostatic charge-discharge experiment was conducted at various current densities between a potential range between 0.0 V and 0.4 V.

## Results and discussion

### Structure analysis

The XRD patterns of the as-synthesized samples are shown in Fig. 1. All diffraction peaks match well with tetragonal-phase Mn<sub>3</sub>O<sub>4</sub> (JCPDS: No. 24-0734), and the observed 14 peaks fit exactly the following Miller indices [21]: (101), (112), (200), (103), (211), (004), (220), (204), (105), (312), (303), (321), (224) and (400), indicating that the as-synthesized Mn<sub>3</sub>O<sub>4</sub> sample was well crystallized and highly pure without other phases. The mean particle diameter can be calculated from the half-peak width of diffraction peaks by the Debye-

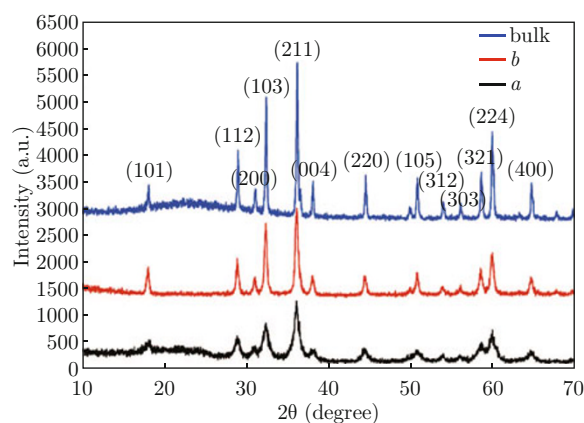


Fig. 1 XRD patterns of the as-synthesized  $\text{Mn}_3\text{O}_4$  nanoparticles and bulk  $\text{Mn}_3\text{O}_4$ .

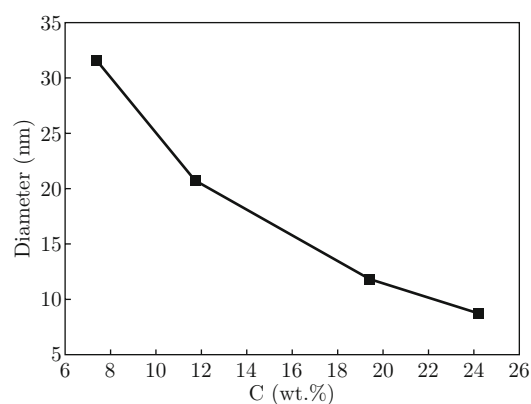


Fig. 2 The relationship between the concentration of Pebax2533 in the isopropanol and average particle diameter of  $\text{Mn}_3\text{O}_4$  nanoparticles.

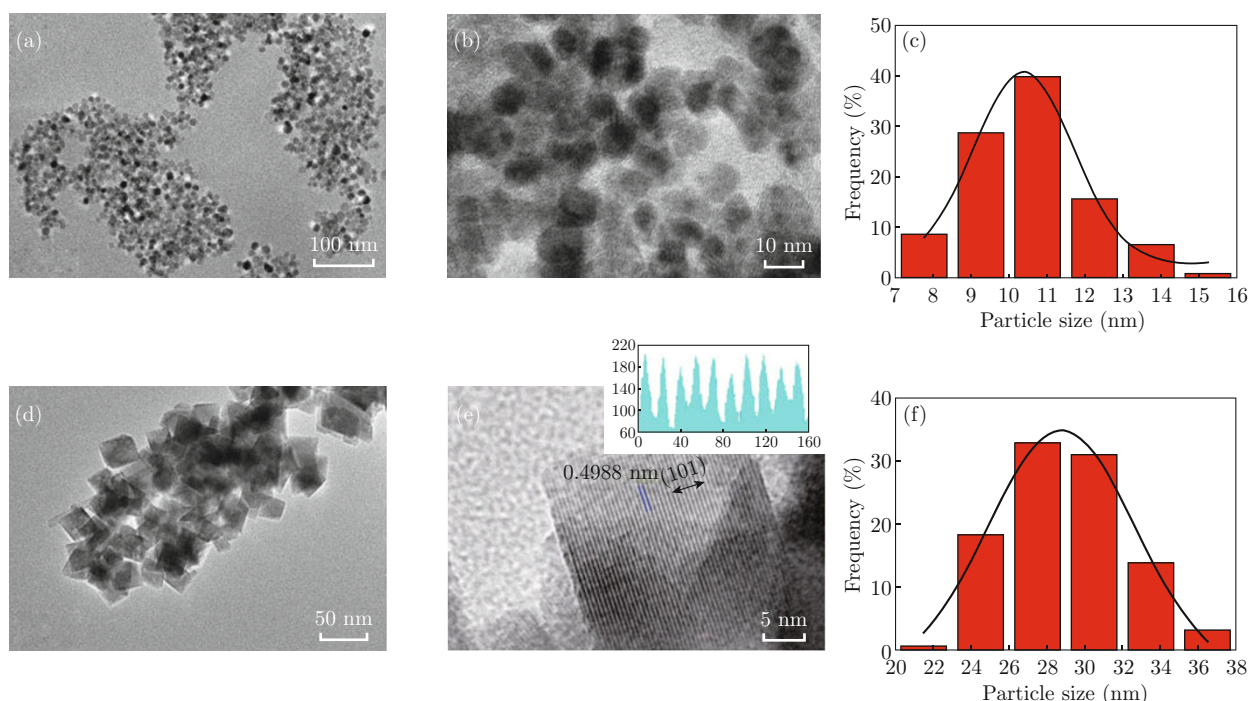


Fig. 3 (a) TEM image, (b) HRTEM image and (c) particle size distribution of sample **a**; (d) TEM image, (e) HRTEM image and (f) particle size distribution of sample **b**.

Scherrer formula. The diameter was 8.7 nm in average for sample **a**, and the corresponding BET area was  $57.9 \text{ m}^2/\text{g}$ . By adjusting the concentration of Pebax2533 in isopropanol, the particle size of nano- $\text{Mn}_3\text{O}_4$  can be well controlled. As shown in Fig. 2, with the decrease of the Pebax2533 concentration, the mean size of  $\text{Mn}_3\text{O}_4$  became larger (the sizes were calculated from the XRD results). Especially, when the concentration of Pebax2533 in isopropanol was 7.4 wt%, nano- $\text{Mn}_3\text{O}_4$  with mean diameter of 31.5 nm was obtained (sample **b** in Fig. 1), and the BET area was  $38.6 \text{ m}^2/\text{g}$ . For comparison, the BET area of bulk  $\text{Mn}_3\text{O}_4$  purchased was

only  $3.8 \text{ m}^2/\text{g}$ , which indicates that the nanoparticles prepared by this method have smaller particle size and higher surface area.

The morphology of the as-synthesized  $\text{Mn}_3\text{O}_4$  sample **a** and sample **b** was investigated by TEM and HRTEM, respectively. As shown in Fig. 3, both of the samples were well dispersed without any aggregation. It was found that sample **a** consisted of spherical particles with mean diameter of about 10.2 nm (Fig. 3(a), 3(b) and 3(c)), while the particle in sample **b** was cubic or octahedral with a size of approximately 28.7 nm (Fig. 3(d), 3(e) and 3(f)). The average size observed

in TEM was in good agreement with the results from XRD. Moreover, the lattice fringes shown in Fig. 3(e) can be ascribed to (101) planes of  $\text{Mn}_3\text{O}_4$  ( $d = 4.988 \text{ \AA}$ ), which agreed well with the lattice parameter obtained from the powder XRD data ( $d = 4.93 \text{ \AA}$ ).

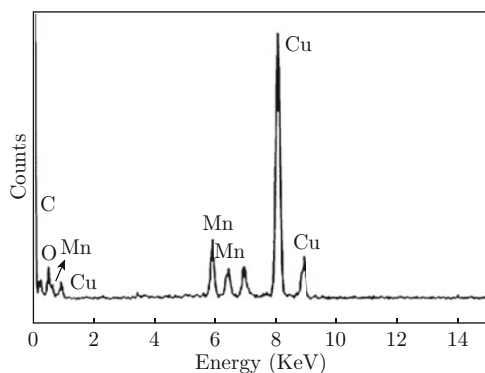


Fig. 4 The EDS spectrum of sample **a**.

The elemental analysis of sample **a** was carried out using energy dispersive spectroscopy (EDS) detector equipped on the TEM. The EDS spectrum was shown in Fig. 4, there were peaks corresponding to four elements: C, O, Cu, and Mn, where C and Cu were from carbon-coated copper grid, and the atomic percentages for Mn and O was 9.75% and 12.74%, respectively, which was very close to the atomic ratio of  $\text{Mn}_3\text{O}_4$ , suggesting that

the obtained nanoparticles were  $\text{Mn}_3\text{O}_4$  in the composition.

In order to analyze the oxidation state of Mn in  $\text{Mn}_3\text{O}_4$  nanoparticles, XPS measurement was performed. As shown in Fig. 5, no impurities were observed on the  $\text{Mn}_3\text{O}_4$  sample except carbon with a survey region of 0-1300 eV [21], and the locations of O 1s, Mn 3s, Mn 2p and Mn 3p were consistent with the results reported in the literature [22]. Moreover, a separation of binding energy was observed between Mn 2p<sub>1/2</sub> and Mn 2p<sub>3/2</sub> levels due to the spin-orbit splitting (Fig. 5(b)). Herein, the spin orbit splitting between the Mn 2p<sub>3/2</sub> (641.07 eV) and Mn 2p<sub>1/2</sub> (652.7 eV) level was 11.63 eV, which perfectly complied with the value of  $\text{Mn}_3\text{O}_4$  reported previously [23].

Pebax copolymers are composed of a hydrophobic polyamide (PA) hard domain and a soft hydrophilic polyether (PE) domain. It has been proposed that the Pebax will form hydrophobic/hydrophilic phase-separated mesostructure under solvothermal conditions, in which PE was periodically distributed within the hydrophobic rigid PA domains [24]. It is preferable for the water-soluble  $\text{Mn}(\text{CH}_3\text{COO})_2$  to locate in the hydrophilic domains, and then it is hydrolyzed by the water coming from alcohol dehydration. After nucleation and growth,  $\text{Mn}_3\text{O}_4$  nanocrystals will be obtained. The principle is schematically shown in Fig. 6.

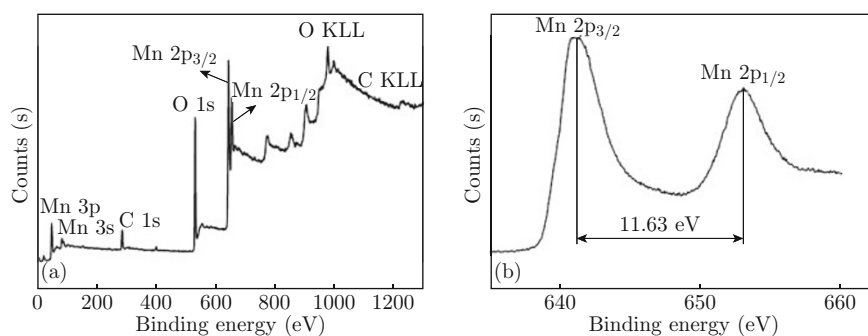


Fig. 5 XPS spectra of (a) survey scan and (b) Mn 2p region of sample **a**.

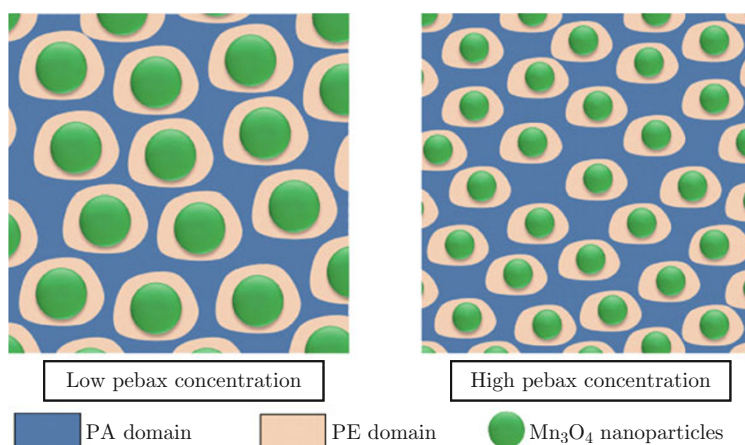


Fig. 6 Schematic illustration of the formation of  $\text{Mn}_3\text{O}_4$  nanoparticles at low and high Pebax concentrations.

In addition, it has been reported that well-connected mesoporous titania was formed under similar conditions [24], whereas we got monodisperse  $\text{Mn}_3\text{O}_4$  nanoparticles in this work. It may be explained from the difference of hydrolysis rate of titanium and manganese precursors. The titanium precursor,  $\text{TiCl}_4$ , is hydrolyzed rapidly, resulting in a sudden formation of nuclei in the system, and then the nuclei grow into small nanocrystals and finally connect with each other. In contrast, the hydrolysis rate of manganese precursor,  $\text{Mn}(\text{CH}_3\text{COO})_2$ , is relatively slower, which causes the slow nucleation and growth rate, and it is in favor of obtaining larger nanoparticles. Furthermore, it has been shown above that smaller  $\text{Mn}_3\text{O}_4$  particles were produced at more concentrated Pebax solutions. When the concentration of Pebax was high, the hydrophilic domains may be compressed and the mass transport in the system gets more sluggish due to the high viscosity, which favors multiple localized nucleation events and therefore promotes smaller nanocrystallites with high surface area.

The concentration of Pebax also has an effect on the morphology of  $\text{Mn}_3\text{O}_4$  nanoparticles. Sample **a** (Pebax concentration is 24.2%) was spherical, while sample **b** was cubic or octahedral (Pebax concentration is 7.4%), indicating that the particle got more faceted with the decrease of Pebax concentration. As mentioned above, the hydrophobic/hydrophilic domain size is different at different Pebax concentration, which probably leads to different growth environment and rate for  $\text{Mn}_3\text{O}_4$  nanoparticles. The low concentration may be in favor of preferential growth of some crystal faces, resulting in  $\text{Mn}_3\text{O}_4$  polyhedrons.

### Electrochemical performances

Cyclic voltammograms (CV) for sample **a**, sample **b** and bulk  $\text{Mn}_3\text{O}_4$  are shown in Fig. 7. The cyclic voltammograms were carried out in a potential range between 0.0 V and 0.6 V in 6 M KOH to evaluate the electrochemical characteristics of the as-synthesized  $\text{Mn}_3\text{O}_4$  nanoparticles. A pair of redox reaction peaks can be seen in the CV curves of each sample, signifying that the capacitance of the  $\text{Mn}_3\text{O}_4$  electrode primarily results from the pseudo capacitance. The following equations were proposed to explain the pseudo-capacitance mechanism of  $\text{Mn}_3\text{O}_4$  in alkaline medium [25],

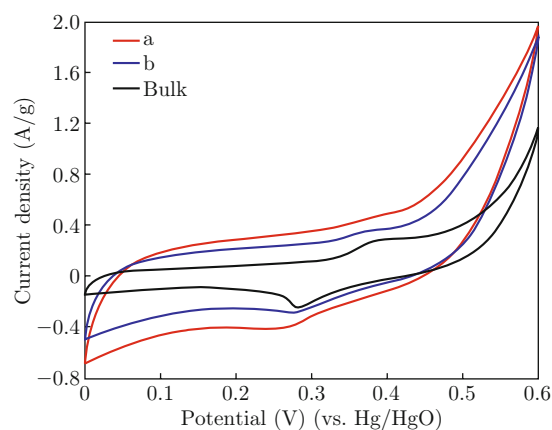
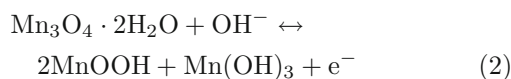
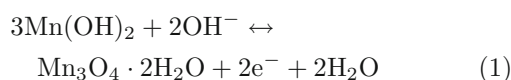


Fig. 7 CV curves of different samples at  $10 \text{ mV s}^{-1}$  in 6 M KOH.

Generally, the capacitance of electrode material is proportional to the area surrounded by the CV curves [26]. As a result, sample **a** presented the highest capacitance as shown in Fig. 7. Furthermore, the CV curves of sample **a** electrode at different scan rates of 10, 30, 50 and  $100 \text{ mV/s}$  were presented in Fig. 8. The increment in current with the scan rate suggested an ideal capacitive behavior [27]. Moreover, there was no significant change in the rectangular shape with increasing scan rates, indicating the electrochemical reversibility of the faraday redox reaction on  $\text{Mn}_3\text{O}_4$  and a good cycle efficiency of the charge-discharge process [28].

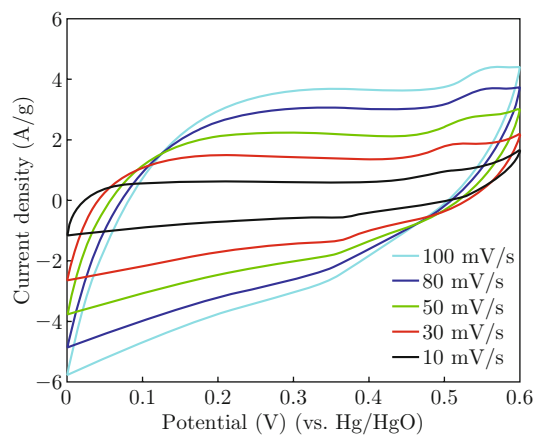


Fig. 8 CV curves of sample **a** in 6 M KOH at different scan rates of 10, 30, 50 and  $100 \text{ mV/s}$ .

The galvanostatic charge-discharge curves of sample **a**, sample **b** and bulk  $\text{Mn}_3\text{O}_4$  is shown in Fig. 9. It can be found that there was slope variation of potential with time in discharge curves, resulted from redox reaction between electrolyte and  $\text{Mn}_3\text{O}_4$  electrode, which was a characteristic of pseudo-capacitive behavior [28]. Additionally, the charge-discharge duration increased in the order of bulk  $\text{Mn}_3\text{O}_4 < \text{sample b} < \text{sample a}$ , which was determined by the specific capacitance of  $\text{Mn}_3\text{O}_4$ .

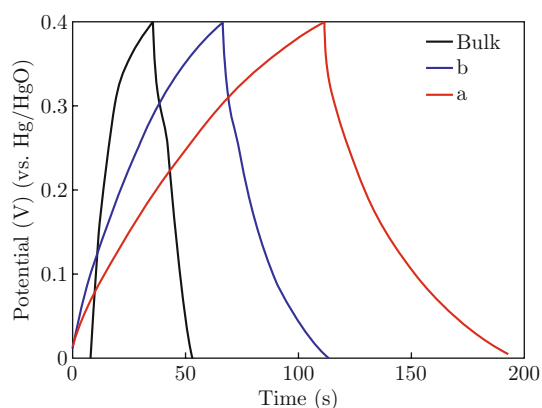


Fig. 9 Galvanostatic charge-discharge curves of different samples at a current density of 1 A/g in 6 M KOH.

The specific capacitance was calculated using the following equation [29],

$$C = \frac{I \times \Delta t}{\Delta V \times m}$$

where  $C$  (F/g) stood for the specific capacitance,  $I$  (A) represented the galvanostatic discharge current,  $\Delta t$  (s) was the discharge time,  $\Delta V$  (V) was the voltage range, and  $m$  (g) was the weight of the active material in the electrode. From Fig. 9, the bulk  $\text{Mn}_3\text{O}_4$  had a specific capacitance of 56.25 F/g at the current density of 1 A/g. In contrast, the specific capacitance for sample **b** was increased to be 137.5 F/g, and sample **a** presented the highest specific capacitance of 202.3 F/g, indicating a significant enhancement of energy capacity. It has been proved that the specific capacitance of electrode was closely related with the specific surface area of active materials [28]. Sample **a** has the smallest particle size, and hence the highest surface area, resulting in the greatest specific capacitance. In comparison, sample **b** and bulk  $\text{Mn}_3\text{O}_4$  showed lower specific capacitance because of the larger particle size. The above result was also in agreement with the surface area derived from the CV measurement (Fig. 7). Additionally, the specific capacitance of sample **a** was larger than that of  $\text{Mn}_3\text{O}_4$  prepared by the microwave-assisted reflux synthesis method [30], which was highly aggregated and usually larger than 50 nm, leading to a lower specific surface area and specific capacitance.

The galvanostatic charge-discharge curves of sample **a** at different current densities are shown in Fig. 10. The calculated specific capacitance of each discharge curve shown in Fig. 10 was 217.5, 202.3, 182.5 and 150.0 F/g at 0.5, 1.0, 2.0 and 5.0 A/g, respectively. The above results indicated that the specific capacitance was reduced with the increase of the charge/discharge current. In comparison with low current, it was more difficult for  $\text{OH}^-$  to fully occupy the active sites at electrode/electrolyte interface at high current, owing

to ions' limited migration velocity and fixed route in the interface, leading to an uncompleted insertion reaction, i.e., more surface of the electrode were inaccessible at high charge/discharge rates, especially for the inner active sites [25]. Thus, the effective redox reaction of  $\text{Mn}_3\text{O}_4$  was limited on the outer surface of electrode, resulting in decreased capacitance.

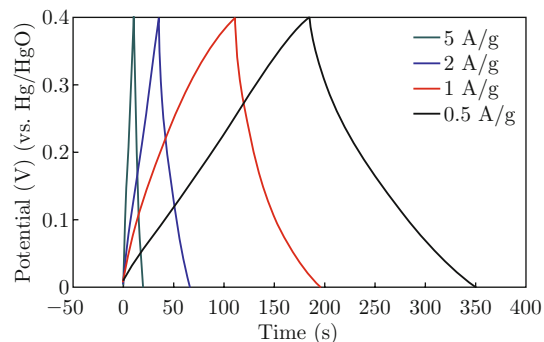


Fig. 10 Galvanostatic charge-discharge curves of sample **a** in 6 M KOH at 0.5, 1.0, 2.0 and 5.0 A/g.

The electrochemical stabilities were investigated by repeating the galvanostatic charge-discharge cycle of sample **a** at a constant current of 1 A  $\text{g}^{-1}$  for 500 cycles in 6 M KOH, and the specific capacitance after every 50 cycles was shown in Fig. 11. It is found that the capacity retained after 500 cycles is about 82% of the initial specific capacitance. These results demonstrated that the  $\text{Mn}_3\text{O}_4$  nanoparticles synthesized were very stable in the repeated charge-discharge cycles as supercapacitor electrode material.

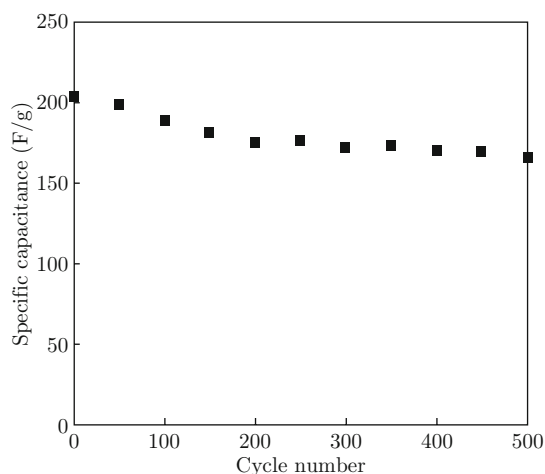


Fig. 11 Dependence of specific capacitance of sample **a** on the number of charge-discharge cycles at 1 A/g in 6 M KOH.

## Conclusions

Monodisperse  $\text{Mn}_3\text{O}_4$  nanoparticles have been synthesized by solvothermal method through self-assembly

using polyether amide block copolymers (Pebax2533) as the template and manganese acetate as the raw material. By adjusting the concentration of Pebax in the precursor, monodisperse single-crystalline  $\text{Mn}_3\text{O}_4$  nanoparticles with diameters in the range between 8.7 and 31.5 nm were prepared. The higher concentration of Pebax in the solution, the smaller  $\text{Mn}_3\text{O}_4$  particles were obtained and higher specific capacitance was presented correspondingly. A capacitance of 217.5 F/g at a current density of 0.5 A/g was obtained on  $\text{Mn}_3\text{O}_4$  nanoparticles with mean diameter of 8.7 nm, which also exhibited good stability and reversibility after 500 continuous charge-discharge cycles. The preparation method for monodisperse single-crystalline  $\text{Mn}_3\text{O}_4$  nanoparticles was simple and low in cost. The template, Pebax, can be recycled. The technique and principles can be extended to the synthesis of other monodisperse oxide nanoparticles of great importance in supercapacitors, catalysis, display, chemical mechanical polishing (CMP), etc.

## Acknowledgements

This work was financially supported by the National Natural Science Foundation of China (No. 21373034), the Specially Hired Professorship-funding of Jiangsu province (No. scz1211400001), and the start-up funds from Changzhou University Jiangsu province, Jiangsu key laboratory of advanced catalytic material and technology, Key laboratory of fine petrochemical engineering and PAPD of Jiangsu Higher Education Institutions.

## References

- [1] B. E. Conway, "Electrochemical supercapacitors scientific fundamentals and technological applications", New York: Plenum Publishers, 1999.
- [2] (a) T. Mei, T. Li, H. Bi, L. Wang, Y. Zhu and Y. T. Qian, "Synthesis and Electrical Capacitance of Carbon Nanoplates", *Eur. J. Inorg. Chem.* 2010(27), 4314-4320 (2010). <http://dx.doi.org/10.1002/ejic.201000387>; (b) B. P. Bastakoti, H. Oveisi, C. C. Hu, K. C. W. Wu, N. Suzuki, K. Takai, Y. Kamachi, M. Imura and Y. Yamauchi, "Mesoporous carbon incorporated with  $\text{In}_2\text{O}_3$  nanoparticles as high-performance supercapacitors", *Eur. J. Inorg. Chem.* 2013(7), 1109-1112 (2013). <http://dx.doi.org/10.1002/ejic.201201311>
- [3] V. V. Pan'kov, "Interaction of (MnZn)O solid solutions with  $\text{Fe}_2\text{O}_3$  as intermediate stage of formation of MnZn ferrites", *Ceram. Int.* 14(2), 87-91 (1988). [http://dx.doi.org/10.1016/S0272-8842\(88\)80003-8](http://dx.doi.org/10.1016/S0272-8842(88)80003-8)
- [4] D. K. Kim, P. Muralidharan, H. W. Lee, R. Ruffo, Y. Yang, C. K. Chan, H. Peng, R. A. Huggins and Y. Cui, "Spinel  $\text{LiMn}_2\text{O}_4$  nanorods as lithium ion battery cathodes", *Nano Lett.* 8(11), 3948-3952 (2008). <http://dx.doi.org/10.1021/nl8024328>
- [5] E. R. Stobbe, B. A. de Boer and J. W. Geus, "The reduction and oxidation behaviour of manganese oxides", *Catal. Today* 47(1-4), 161-167 (1999). [http://dx.doi.org/10.1016/S0920-5861\(98\)00296-X](http://dx.doi.org/10.1016/S0920-5861(98)00296-X)
- [6] E. J. Grootendorst, Y. Verbeek and V. Ponec, "The role of the Mars and Van Krevelen mechanism in the selective oxidation of nitrosobenzene and the deoxygenation of nitrobenzene on oxidic catalysts", *J. Catal.* 157(2), 706-712 (1995). <http://dx.doi.org/10.1006/jcat.1995.1336>
- [7] W. S. Kijlstra, J. C. M. L. Daamen, J. M. van de Graaf, B. van der Linden, E. K. Poels and A. Blik, "Inhibiting and deactivating effects of water on the selective catalytic reduction of nitric oxide with ammonia over  $\text{MnO}_x/\text{Al}_2\text{O}_3$ ", *Appl. Catal. B-Environ.* 7(3-4), 337-357 (1996). [http://dx.doi.org/10.1016/0926-3373\(95\)00052-6](http://dx.doi.org/10.1016/0926-3373(95)00052-6)
- [8] (a) Z. Chen, J. K. L. Lai and C. H. Shek, "Evolution of electronic structure and spectral evaluation in single-crystal  $\text{Mn}_3\text{O}_4$  nanorods", *J. Chem. Phys.* 124(18), 184707-5 (2006). <http://dx.doi.org/10.1063/1.2199848>; (b) J. W. Lee, A. S. Hall, J. D. Kim and T. E. Mallouk, "A facile and template-free hydrothermal synthesis of  $\text{Mn}_3\text{O}_4$  nanorods on graphene sheets for supercapacitor electrodes with long cycle stability", *Chem. Mater.* 24(6), 1158-1164 (2012). <http://dx.doi.org/10.1021/cm203697w>; (c) D. Wang, Y. Li, Q. Wang and T. Wang, "Facile synthesis of porous  $\text{Mn}_3\text{O}_4$  nano-crystal-graphene nanocomposites for electrochemical supercapacitors", *Eur. J. Inorg. Chem.* 2012(4), 628-635 (2012). <http://dx.doi.org/10.1002/ejic.201100983>
- [9] Y. Q. Chang, X. Y. Xu, X. H. Luo, C. P. Chen and D. P. Yu, "Synthesis and characterization of  $\text{Mn}_3\text{O}_4$  nanoparticles", *J. Cryst. Growth* 264(1-3), 232-236 (2004). <http://dx.doi.org/10.1016/j.jcrysgro.2003.11.11>
- [10] Y. Hu, J. Chen, X. Xue and T. Li, "Synthesis of monodispersed single-crystal compass-shaped  $\text{Mn}_3\text{O}_4$  via gamma-ray irradiation", *Mater. Lett.* 60(3), 383-385 (2006). <http://dx.doi.org/10.1016/j.matlet.2005.08.056>
- [11] P. Z. Si, E. Brück, Z. D. Zhang, O. Tegus, W. S. Zhang, K. H. J. Buschow and J. C. P. Klaasse, "Structural and magnetic properties of Mn nanoparticles prepared by arc-discharge", *Mater. Res. Bull.* 40(1), 29-37 (2005). <http://dx.doi.org/10.1016/j.materresbull.2004.09.010>
- [12] W. X. Zhang, C. Wang, X. M. Zhang, Y. Xie and Y. T. Qian, "Low temperature synthesis of nanocrystalline  $\text{Mn}_3\text{O}_4$  by a solvothermal method", *Solid State Ionics* 117(3-4), 331-335 (1999). [http://dx.doi.org/10.1016/S0167-2738\(98\)00432-9](http://dx.doi.org/10.1016/S0167-2738(98)00432-9)
- [13] S. Ardizzone, C. L. Bianchi and D. Tirelli, " $\text{Mn}_3\text{O}_4$  and  $\gamma\text{-MnOOH}$  powders, preparation, phase composition and XPS characterisation", *Colloid. Surface. A*

- 134(3), 305-312 (1998). [http://dx.doi.org/10.1016/S0927-7757\(97\)00219-7](http://dx.doi.org/10.1016/S0927-7757(97)00219-7)
- [14] (a) F. H. Schacher, P. A. Rupar and I. Manners, "Functional block copolymers: nanostructured materials with emerging applications", *Angew. Chem. Int. Edit.* 51(32), 7898-7921 (2012). <http://dx.doi.org/10.1002/anie.201200310>; (b) Y. Mai and A. Eisenberg, "Selective localization of preformed nanoparticles in morphologically controllable block copolymer aggregates in solution", *Accounts Chem. Res.* 45(10), 1657-1666 (2012). <http://dx.doi.org/10.1021/ar2003144>
- [15] (a) Y. Li, H. Tan, X. X. Yang, B. Goris, J. Verbeeck, S. Bals, P. Colson, R. Cloots, G. Van Tendeloo and B. L. Su, "Well shaped  $Mn_3O_4$  nano-octahedra with anomalous magnetic behavior and enhanced photodecomposition properties", *Small* 7(4), 475-483 (2011). <http://dx.doi.org/10.1002/smll.201001403>; (b) W. Wang, T. Yang, G. Yan and H. Li, "Synthesis of  $Mn_3O_4$  hollow octahedrons and their possible growth mechanism", *Mater. Lett.* 82, 237-239 (2012). <http://dx.doi.org/10.1016/j.matlet.2012.05.070>; (c) K. An, M. Park, J. H. Yu, H. B. Na, N. Lee, J. Park, S. H. Choi, I. C. Song, W. K. Moon and T. Hyeon, "Synthesis of uniformly sized manganese oxide nanocrystals with various sizes and shapes and characterization of their T1 magnetic resonance relaxivity", *Eur. J. Inorg. Chem.* 2012(12), 2148-2155 (2012). <http://dx.doi.org/10.1002/ejic.201101193>; (d) M. Liu and H. C. Zeng, "Spontaneous formations of superlattices and supracrystals from various forms of  $Mn_3O_4$  nanocrystals", *Cryst. Growth Des.* 12(11), 5561-5570 (2012). <http://dx.doi.org/10.1021/cg3011103>
- [16] X. Ren, J. Ren, H. Li, S. Feng and M. Deng, "Poly (amide-6-b-ethylene oxide) multilayer composite membrane for carbon dioxide separation", *Int. J. Greenh. Gas Con.* 8, 111-120 (2012). <http://dx.doi.org/10.1016/j.ijggc.2012.01.017>
- [17] N. L. Le, Y. Wang and T. S. Chung, "Pebax/POSS mixed matrix membranes for ethanol recovery from aqueous solutions via pervaporation", *J. Membrane Sci.* 379(1-2), 174-183 (2011). <http://dx.doi.org/10.1016/j.memsci.2011.05.060>
- [18] E. Tocci, L. D. Lorenzo, A. Gugliuzza, M. Macchione and E. Drioli, "Pure and modified Co-poly(amide-12-b-ethylene oxide) membranes for gas separation studied by molecular investigations", *AIP Conf. Proc.* 1298(1), 724-727 (2010). <http://dx.doi.org/10.1063/1.3516418>
- [19] T. Kamal, S. Y. Park, J. H. Park and Y. W. Chang, "Structural evolution of poly(ether-b-amide12) elastomers during the uniaxial stretching: An in situ wide-angle X-ray scattering study", *Macromol. Res.* 20(7), 725-731 (2012). <http://dx.doi.org/10.1007/s13233-012-0109-z>
- [20] A. Moses Ezhil Raj, S. G. Victoria, V. B. Jothy, C. Ravidhas, J. Wollschläger, M. Suendorf, M. Neumann, M. Jayachandran and C. Sanjeeviraja, "XRD and XPS characterization of mixed valence  $Mn_3O_4$  hausmanite thin films prepared by chemical spray pyrolysis technique", *Appl. Surf. Sci.*, 256(9), 2920-2926 (2010). <http://dx.doi.org/10.1016/j.apsusc.2009.11.051>
- [21] M. Oku, K. Hirokawa and S. Keda, "X-ray photoelectron spectroscopy of manganese-oxygen systems", *J. Electron Spectrosc.* 7(5), 465-473 (1975). [http://dx.doi.org/10.1016/0368-2048\(75\)85010-9](http://dx.doi.org/10.1016/0368-2048(75)85010-9)
- [22] J. S. Foord, R. B. Jackman and G. C. Allen, "An X-ray photoelectron spectroscopic investigation of the oxidation of manganese", *Philos. Mag. A* 49(5), 657-663 (1984). <http://dx.doi.org/10.1080/01418618408233293>
- [23] Y. Fan, X. Zhang, Y. Liu, Q. Cai and J. Zhang, "One-pot hydrothermal synthesis of  $Mn_3O_4$ /graphene nanocomposite for supercapacitors", *Mater. Lett.* 95,153-156 (2013). <http://dx.doi.org/10.1016/j.matlet.2012.12.110>
- [24] X. M. Jiang and C. J. Brinker, "Rigid templating of high surface-area, mesoporous, nanocrystalline rutile using a polyether block amide copolymer template", *Chem. Commun.* 46(33), 6123-6125 (2010). <http://dx.doi.org/10.1039/C0CC01394C>
- [25] L. X. Zhu, S. Zhang, Y. H. Cui, H. H. Song and X. H. Chen, "One step synthesis and capacitive performance of grapheme nanosheets/ $Mn_3O_4$  composite", *Electrochim. Acta* 89, 18-23 (2013). <http://dx.doi.org/10.1016/j.electacta.2012.10.157>
- [26] Michio Inagaki, Hidetaka Konno and Osamu Tanaike, "Carbon materials for electrochemical capacitors", *J. Power Sources* 195(24), 7880-7903 (2010). <http://dx.doi.org/10.1016/j.jpowsour.2010.06.036>
- [27] S. Nagamuthu, S. Vijayakumar and G. Muralidharan, "Synthesis of  $Mn_3O_4$ /Amorphous carbon nanoparticles as electrode material for high performance supercapacitor applications", *Energ. Fuel.* 27(6), 3508-3515 (2013). <http://dx.doi.org/10.1021/ef400212b>
- [28] D. P. Dubal and R. Holze, "Self-assembly of stacked layers of  $Mn_3O_4$  nanosheets using a scalable chemical strategy for enhanced, flexible, electrochemical energy storage", *J. Power Sources* 238, 274-282 (2013). <http://dx.doi.org/10.1016/j.jpowsour.2013.01.198>
- [29] Y. Z. Wu, S. Q. Liu, H. Y. Wang, X. W. Wang, X. Zhang and G. H. Jin, "A novel solvothermal synthesis of  $Mn_3O_4$ /grapheme composites for supercapacitors", *Electrochim. Acta* 90, 210-218 (2013). <http://dx.doi.org/10.1016/j.electacta.2012.11.124>
- [30] K. Sankar, D. Kalpana and R. Selvan, "Electrochemical properties of microwave-assisted reflux-synthesized  $Mn_3O_4$  nanoparticles in different electrolytes for supercapacitor applications", *J. Appl. Electrochem.* 42(7), 463-470 (2012). <http://dx.doi.org/10.1007/s10800-012-0424-2>